

Model dependence of single-energy fits to pion photoproduction data

Ron L. Workman, Mark W. Paris, William J. Briscoe,^a
Lothar Tiator, Sven Schumann, Michael Ostrick^b,
and Sabit S. Kamalov^c

^a*Center for Nuclear Studies, Department of Physics,
The George Washington University, Washington, D.C. 20052*

^b*Institut für Kernphysik, Johannes Gutenberg Universität, D-55099, Mainz, Germany*

^c*Bogoliubov Laboratory for Theoretical Physics, JINR Dubna, 141980 Moscow Region, Russia*

(Dated: November 2, 2018)

Model dependence of multipole analysis has been explored through energy-dependent and single-energy fits to pion photoproduction data. The MAID energy-dependent solution has been used as input for an event generator producing realistic pseudo data. These were fitted using the SAID parametrization approach to determine single-energy and energy-dependent solutions over a range of lab photon energies from 200 to 1200 MeV. The resulting solutions were found to be consistent with the input amplitudes from MAID. Fits with a χ -squared per datum of unity or less were generally achieved. We discuss energy regions where consistent results are expected, and explore the sensitivity of fits to the number of included single- and double-polarization observables. The influence of Watson's theorem is examined in detail.

PACS numbers: 11.80.Et, 25.20.Lj, 29.85.Fj, 13.60.Le

I. INTRODUCTION

The non-perturbative regime of quantum chromodynamics (QCD) is characterized by an array of hadronic resonances. The gross features of this spectrum have been understood theoretically within the context of constituent quark models. Experimentally, measurements of reaction observables from an array of collision processes, in particular pion photoproduction, have shown the limitations of the quark model description. Precision electromagnetic facilities around the world have begun to give a more detailed picture of the hadronic resonances, particularly for the resonances of the nucleon, and ushered in a renaissance in the field of hadronic reaction theory.

Crucial to this program is the determination of reaction amplitudes from experimental observables. Model independent extraction of reaction amplitudes in both spin (*eg.* CGLN, helicity, transversity, ...) and partial-wave bases is a well-studied yet complex task. Typically, coupled-channel models based on Lagrangians of hadronic effective field theory involve hundreds of bare parameters in order to obtain realistic descriptions of data covering the first, second, and third resonance regions. Complementary to this approach is the extraction of amplitudes with smaller numbers of parameters and minimal model dependence.

Two types of analysis, typically performed in parametrizing the reaction amplitudes, lead to energy dependent (ED) or global solutions and energy independent or single-energy (SE) solutions. The SE amplitudes, generally extracted through the partial-wave analysis of scattering or reaction data, are often used as the starting point for more involved multi-channel analyses [1]. The term *data* is commonly applied to these sets of amplitudes, implying a relatively model-independent link to the underlying experimental data. This approach has

been successful for some hadronic and nuclear collision processes. For example, complete or nearly complete sets of data have been assembled over restricted kinematic regions for nucleon-nucleon [2] and pion-nucleon [3] elastic scattering. These have allowed a formal study of the ambiguities associated with the amplitude reconstruction process and yielded a set of useful amplitudes[4] employed, for example, in the determination of the isospin $\frac{1}{2} N$ and isospin- $\frac{3}{2} \Delta$ nucleon resonances[5].

In pion photoproduction, which is the focus of the present study, SE solutions are generally determined from data within a narrow range of energies, with less than the number of observables required for a direct, unique amplitude reconstruction. In order to obtain a stable solution, further constraints are required. Generally, the SE solutions or fits are constrained by the results of a global ED fit. Below, we will discuss how the ED and SE fits are related, and how this procedure differs from amplitude reconstruction.

Multipole fits from the MAID and SAID groups have been updated to include improved measurements as they have become available. Both ED and SE results have been presented and some multipoles show significant differences. In order to avoid the influence of systematic uncertainties in the database, as a potential source of these discrepancies, we have generated pseudo data based on the MAID and SAID ED fits. Multipoles extracted from these idealized datasets show much less variation than is seen in fits to the existing experimental datasets. Below we compare multipoles analyzed using the two different techniques, ED and SE, and suggest energy ranges over which varying degrees of model independence can be expected.

In the next section, we provide information sufficient to fix the phase and sign conventions of amplitudes and observables. It is important to note that the phase and

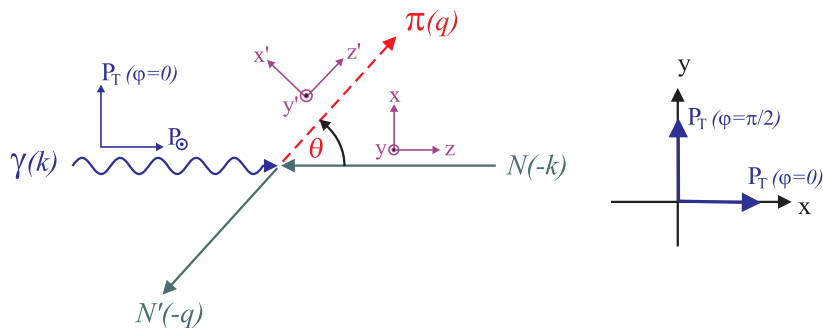


FIG. 1: Frames for polarization vectors in the CM.

sign conventions adopted by the MAID and SAID groups have been consistent for many years and, as such, have been adopted by a large number of experimental groups. Recent publications[6, 7], however, have departed from this convention and we offer the complete set of equations in Sec.II in order to facilitate comparisons.

Section III describes the approaches taken by the SAID and MAID groups in the determination of SE solutions. In the following section, Sec. IV, we describe the event generator used to produce the pseudo data employed in the SE and ED fits. The results of our fits are given in a comparison of observables and multipole amplitudes in Sec.V. Our ED and SE solutions span a range of lab photon energies E_γ from 200 to 1200 MeV or total CM energies W from 1120 to 1770 MeV. In order to limit the length of this article, we have included figures for lab photon energies of 340 and 600 MeV corresponding to CM energies of 1230 and 1420 MeV. The lower energy is in the region dominated by the elastic P_{33} partial wave. The higher energy is characterized generally by the onset of larger inelasticities, except in the P_{33} partial wave. Section VI gives a discussion of the results and our conclusions.

II. AMPLITUDES AND OBSERVABLES

In general, pion photoproduction from the nucleon, $\gamma N \rightarrow \pi N$, is expressed by four invariant amplitudes, A_i , which are covariant functions of two kinematical variables, such as the Mandelstam variables s, t , or more often E_γ, θ , the photon laboratory energy and the pion CM angle. For given initial and final spin states i, f the transition matrix element is given by

$$t_{\pi\gamma}^{fi} = \bar{u}(p_f) \sum_{k=1}^4 A_k \varepsilon_\mu M_k^\mu u(p_i) \quad (1)$$

where $u_{f,(i)}(p)$ is the Dirac spinor of the final (initial) nucleon, normalized as $\bar{u}(p)u(p) = 2M_N$, ε_μ is the polarization vector of the photon, and M_k^μ are a set of Dirac matrices defined to be consistent with Ref.[8]. This leads

to the exclusive photoproduction cross section

$$\frac{d\sigma^{f,i}}{d\Omega} = \frac{q}{k} \left(\frac{M_N}{4\pi W} \right)^2 |t_{\pi\gamma}^{fi}|^2, \quad (2)$$

where $q(k)$ is the magnitude of the three-momentum of the pion (photon), M_N is the mass of the nucleon, W is the CM scattering energy, and $t_{\pi\gamma}^{fi}$ is the transition matrix element for pion photoproduction; the spin and internal quantum numbers in this expression are implied. This matrix element is simply expressed in terms of the Pauli spinors of the initial and final state nucleons.

A. CGLN and Helicity Amplitudes

Expressed in terms of two-dimensional Pauli spinors, the matrix element of the electromagnetic current takes the form

$$t_{\pi\gamma}^{fi} = -\frac{4\pi W}{M_N} \chi_f^\dagger \mathcal{F} \chi_i, \quad (3)$$

where $\chi_{f(i)}$ is a Pauli spinor for the nucleon in final (initial) state. Following Ref.[8], the operator \mathcal{F} is decomposed into four component amplitudes, F_i , called the ‘‘CGLN’’ amplitudes, as

$$\begin{aligned} \mathcal{F} &= -\epsilon_\mu J_{\pi N}^\mu \\ &= i(\vec{\sigma} \cdot \hat{\epsilon}) F_1 + (\vec{\sigma} \cdot \hat{q})(\vec{\sigma} \times \hat{k}) \cdot \hat{\epsilon} F_2 \\ &\quad + i(\hat{\epsilon} \cdot \hat{q})(\vec{\sigma} \cdot \hat{k}) F_3 + i(\hat{\epsilon} \cdot \hat{q})(\vec{\sigma} \cdot \hat{q}) F_4 \end{aligned} \quad (4)$$

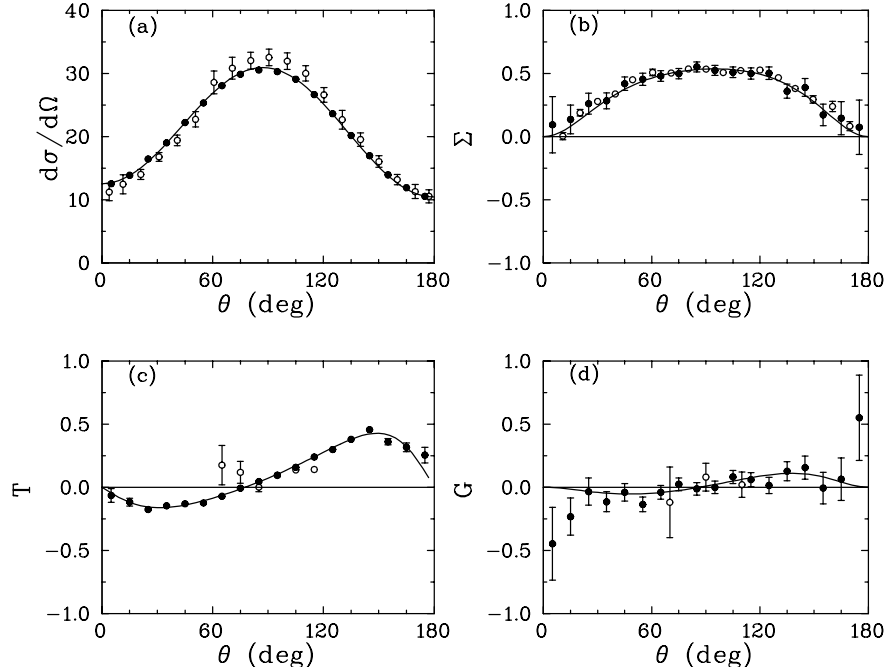


FIG. 2: Pseudo data (black circles) compared to published experimental data (open circles) and the MAID ED solution MD07 (solid curve) at photon beam energies of 320 MeV for $d\sigma/d\Omega$ (a), Σ (b) and T (c) and 340 MeV for the double spin observable G (d).

where $\epsilon^\mu = (0, \vec{\epsilon})$ and $\vec{\epsilon} \cdot \vec{k} = 0$ for real photons. The multipole series of the CGLN amplitudes takes the form[8, 9]:

$$F_1 = \sum_{l=0}^{\infty} [(lM_{l+} + E_{l+}) P'_{l+1}(x) + ((l+1)M_{l-} + E_{l-}) P'_{l-1}(x)], \quad (5)$$

$$F_2 = \sum_{l=1}^{\infty} [(l+1)M_{l+} + lM_{l-}] P'_l(x), \quad (6)$$

$$F_3 = \sum_{l=1}^{\infty} [(E_{l+} - M_{l+}) P''_{l+1}(x) + (E_{l-} + M_{l-}) P''_{l-1}(x)], \quad (7)$$

$$F_4 = \sum_{l=2}^{\infty} [M_{l+} - E_{l+} - M_{l-} - E_{l-}] P''_l(x), \quad (8)$$

where $x = \cos \theta$ is the cosine of the scattering angle.

The representation of the photoproduction amplitudes given by Eqs.(4)–(8) is useful in determining a consistent notation since the CGLN amplitudes take this form in the literature universally, to our knowledge. This provides a context for the discussion of sign or phase conventions and various linear combinations of amplitudes to form different bases. In this way, one may readily discriminate various sign conventions used for observables.

While more compact expressions for the observables of Eqs.(17)–(32), can be given in terms of the helicity or transversity amplitudes (see Table I), these amplitudes are not uniquely defined. Differing phases and varying linear combinations to define the helicity and transversity bases have been used in the literature. In this work, we use the conventions adopted by Walker[10] for the helicity amplitudes. These conventions are also used in Refs.[11, 12] of Barker, Donnachie, Storrow (BDS). The relations in Table I give the reaction observables explicitly in terms of the helicity amplitudes using the conventions of Ref.[10]. Comparisons are made there to works using differing sign conventions for convenience.

The helicity amplitudes are related to the CGLN amplitudes as

$$H_1 = -\frac{1}{\sqrt{2}} \sin \theta \cos \frac{\theta}{2} (F_3 + F_4), \quad (9)$$

$$H_2 = \sqrt{2} \cos \frac{\theta}{2} [(F_2 - F_1) + \frac{1 - \cos \theta}{2} (F_3 - F_4)], \quad (10)$$

$$H_3 = \frac{1}{\sqrt{2}} \sin \theta \sin \frac{\theta}{2} (F_3 - F_4), \quad (11)$$

$$H_4 = \sqrt{2} \sin \frac{\theta}{2} [(F_1 + F_2) + \frac{1 + \cos \theta}{2} (F_3 + F_4)], \quad (12)$$

which are identical to Eqs.(24) of Ref.[10]. The outgoing pion direction is specified by the scattering angle θ and

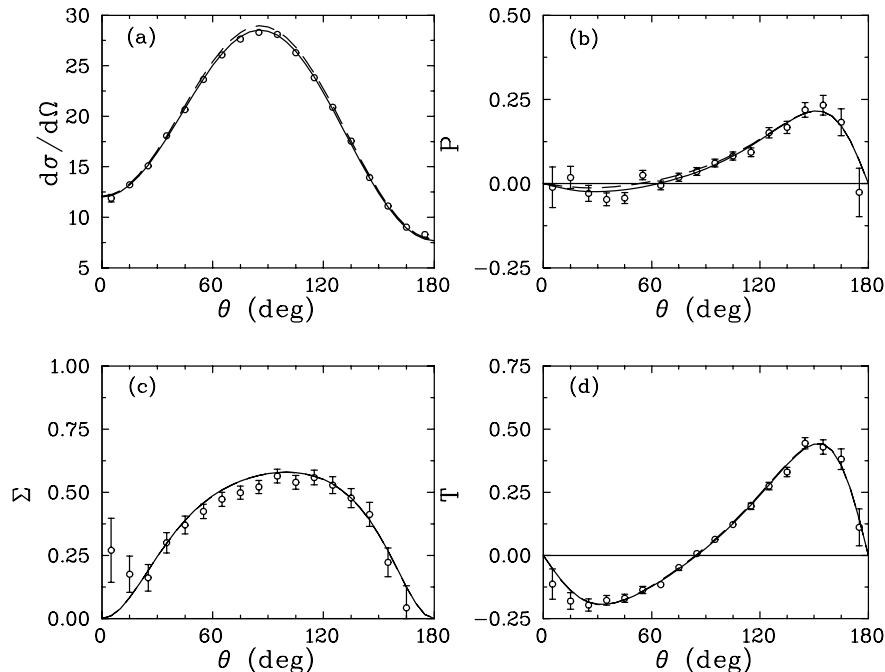


FIG. 3: The SE4 fit (solid) and ED4 fit (dashed) compared to pseudo data (open circles) generated from MD07 for the $\pi^0 p$ channel for observables $d\sigma/d\Omega$ (a), P (b), Σ (c), and T (d), at $E_\gamma = 340$ MeV. Each figure includes two, usually overlapping, curves.

azimuthal angle ϕ . We have chosen $\phi = 0$ by aligning the coordinate system with the reaction plane as in Fig.(1) (see the discussion immediately following Eq.(16) below). The same helicity amplitudes are employed by BDS[11, 12] with, however, a distinct naming convention:

$$\begin{aligned} S_1 &= H_1, & N &= H_2, \\ D &= H_3, & S_2 &= H_4. \end{aligned} \quad (13)$$

B. Coordinate Frames and Polarizations

Experiments with three types of polarization may be performed in meson photoproduction: photon beam polarization, polarization of the target nucleon, and polarization of the recoil nucleon. The target polarization is described in the frame $\{x, y, z\}$ of Fig.(1), with the z -axis coincident with the photon momentum \hat{k} , the y -axis perpendicular to the reaction plane, $\hat{y} = \hat{k} \times \hat{q} / \sin \theta$, and the x -axis given by $\hat{x} = \hat{y} \times \hat{z}$. For recoil polarization we use the frame $\{x', y', z'\}$, with the z' -axis coincident with the momentum of the outgoing meson \hat{q} , the y' -axis coincident with the y -axis, as for the target polarization, and the x' -axis given by $\hat{x}' = \hat{y}' \times \hat{z}'$.

The photon polarization is either linear or circular. A linearly polarized photon is defined by the degree of

transverse polarization, P_T , and the angle φ of the polarization plane relative to the reaction plane or, equivalently, to the \hat{x} direction. For example, a beam completely polarized in the reaction plane has $\varphi = 0$ (with $P_T = 1$); for a beam polarized perpendicular to the reaction plane, \hat{y} , the polarization angle is $\varphi = \pi/2$ (with $P_T = 1$). For a photon of right-(left-)circular polarization $P_\odot = \pm 1$.

The target nucleon polarization is specified by three polarization components (P_x, P_y, P_z) with respect to the $(\hat{x}, \hat{y}, \hat{z})$ coordinate system, displayed in Fig.(1). The recoil nucleon polarization is specified similarly by $(P_{x'}, P_{y'}, P_{z'})$ with respect to $(\hat{x}', \hat{y}', \hat{z}')$ also shown in Fig.(1).

C. Polarization Observables

We may classify the differential cross section for general polarization states of the beam, target, and recoil particles by three classes of double polarization experiments. Using the notation described in the previous subsection, measurements with polarized photons and a polarized target, the *beam-target* experiments, are given

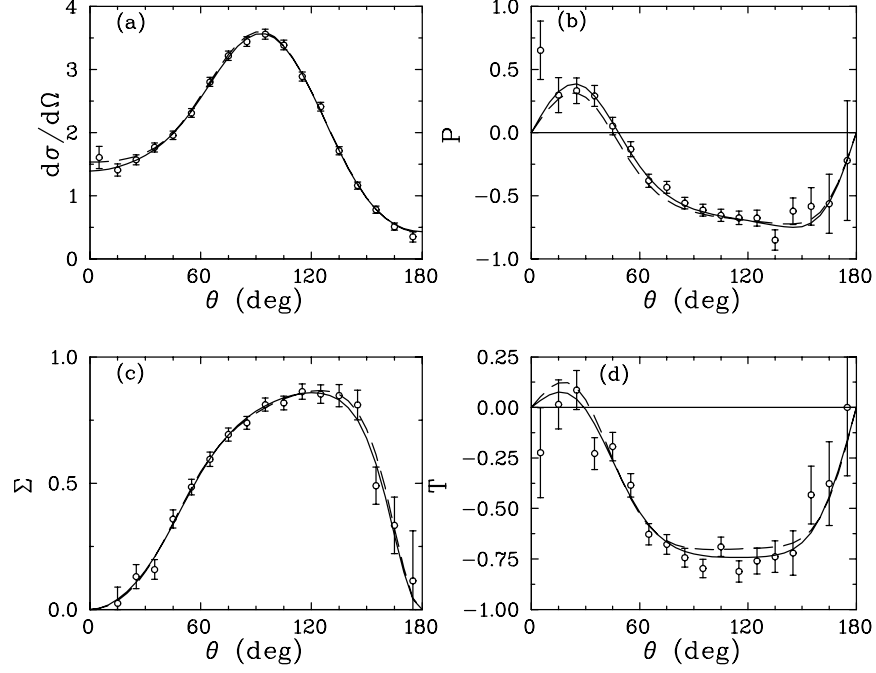


FIG. 4: The SE4 fit (solid) and ED4 (dashed) compared to pseudo data (open circles) for $\pi^0 p$ at 600 MeV, as in Fig.(3).

by the differential cross section

$$\begin{aligned} \frac{1}{\sigma_0} \frac{d\sigma}{d\Omega} &= 1 - P_T \Sigma \cos 2\varphi \\ &+ P_x (-P_T H \sin 2\varphi + P_\odot F) \\ &+ P_y (T - P_T P \cos 2\varphi) \\ &+ P_z (P_T G \sin 2\varphi - P_\odot E); \end{aligned} \quad (14)$$

for polarized photons and measured recoil polarization, *beam-recoil* experiments, we obtain

$$\begin{aligned} \frac{1}{\sigma_0} \frac{d\sigma}{d\Omega} &= 1 - P_T \Sigma \cos 2\varphi \\ &+ P_{x'} (-P_T O_{x'} \sin 2\varphi - P_\odot C_{x'}) \\ &+ P_{y'} (P - P_T T \cos 2\varphi) \\ &+ P_{z'} (-P_T O_{z'} \sin 2\varphi - P_\odot C_{z'}); \end{aligned} \quad (15)$$

for the polarized target and recoil polarization measurements, *target-recoil* experiments:

$$\begin{aligned} \frac{1}{\sigma_0} \frac{d\sigma}{d\Omega} &= 1 + P_y T + P_{y'} P + P_{x'} (P_x T_{x'} - P_z L_{x'}) \\ &+ P_{y'} P_y \Sigma + P_{z'} (P_x T_{z'} + P_z L_{z'}). \end{aligned} \quad (16)$$

In these equations, σ_0 denotes the unpolarized differential cross section. Here φ is the azimuthal angle of the photon polarization vector with respect to the reaction plane. Alternatively, one could fix the photon polarization vector and observe the pion out of the polarization plane of the photon. In this case one would obtain a pion angle $\phi = -\varphi$. This leads to a minus sign in all terms proportional to $\sin 2\varphi$. Equations (14), (15), and (16) are identical with Eqs.(2), (3), and (4) of Ref.[12] upon conversion of their $\sigma_i \rightarrow P_{i'}$, $O_i \rightarrow O_{i'}$, $C_i \rightarrow C_{i'}$, $T_i \rightarrow T_{i'}$, and $L_i \rightarrow L_{i'}$. Note, however, that our coordinate frames are identical to those of BDS. The triple polarization cross section, which specifies the polarizations of the beam, target, and recoil nucleon simultaneously, provides no additional information in the pion photoproduction reaction.

The spin observables, expressed in terms of the CGLN amplitudes, within the sign convention of Barker, Donachie and Storrow, have been consistently employed in both the MAID and SAID parametrizations. They are given explicitly as:

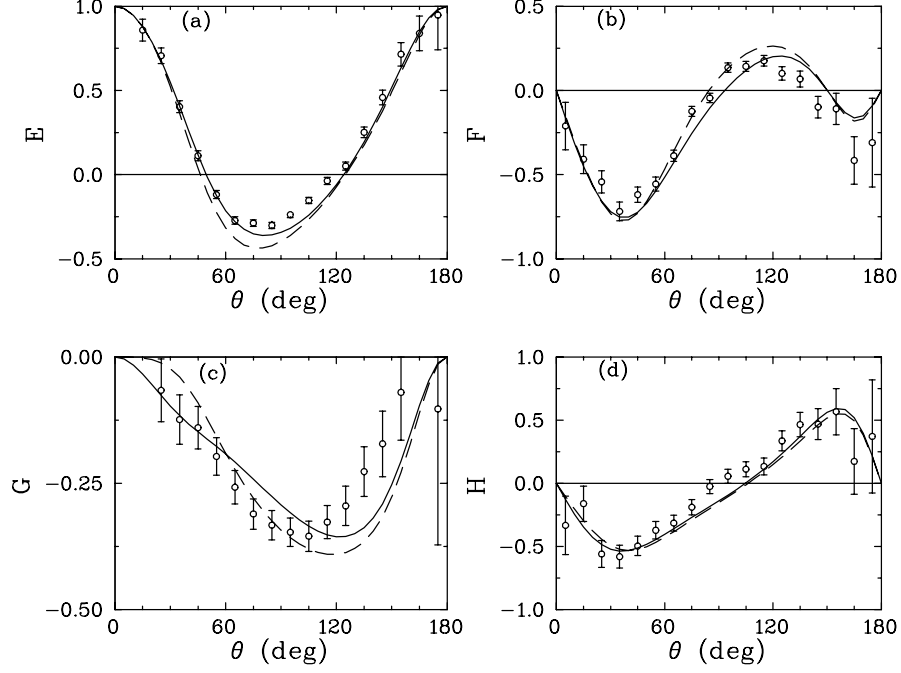


FIG. 5: The SE4 fit (solid) and ED4 (dashed) compared to pseudo data (open circles) for $\pi^0 p$ beam-target observables, E (a), F (b), G (c), and H (d) at 600 MeV.

$$\sigma_0 = \text{Re} \{ F_1^* F_1 + F_2^* F_2 + \sin^2 \theta (F_3^* F_3 / 2 + F_4^* F_4 / 2 + F_2^* F_3 + F_1^* F_4 + \cos \theta F_3^* F_4) - 2 \cos \theta F_1^* F_2 \} \rho \quad (17)$$

$$\hat{\Sigma} = -\sin^2 \theta \text{Re} \{ (F_3^* F_3 + F_4^* F_4) / 2 + F_2^* F_3 + F_1^* F_4 + \cos \theta F_3^* F_4 \} \rho \quad (18)$$

$$\hat{T} = \sin \theta \text{Im} \{ F_1^* F_3 - F_2^* F_4 + \cos \theta (F_1^* F_4 - F_2^* F_3) - \sin^2 \theta F_3^* F_4 \} \rho \quad (19)$$

$$\hat{P} = -\sin \theta \text{Im} \{ 2F_1^* F_2 + F_1^* F_3 - F_2^* F_4 - \cos \theta (F_2^* F_3 - F_1^* F_4) - \sin^2 \theta F_3^* F_4 \} \rho \quad (20)$$

$$\hat{E} = \text{Re} \{ F_1^* F_1 + F_2^* F_2 - 2 \cos \theta F_1^* F_2 + \sin^2 \theta (F_2^* F_3 + F_1^* F_4) \} \rho \quad (21)$$

$$\hat{F} = \sin \theta \text{Re} \{ F_1^* F_3 - F_2^* F_4 - \cos \theta (F_2^* F_3 - F_1^* F_4) \} \rho \quad (22)$$

$$\hat{G} = \sin^2 \theta \text{Im} \{ F_2^* F_3 + F_1^* F_4 \} \rho \quad (23)$$

$$\hat{H} = \sin \theta \text{Im} \{ 2F_1^* F_2 + F_1^* F_3 - F_2^* F_4 + \cos \theta (F_1^* F_4 - F_2^* F_3) \} \rho \quad (24)$$

$$\hat{C}_{x'} = \sin \theta \text{Re} \{ F_1^* F_1 - F_2^* F_2 - F_2^* F_3 + F_1^* F_4 - \cos \theta (F_2^* F_4 - F_1^* F_3) \} \rho \quad (25)$$

$$\hat{C}_{z'} = \text{Re} \{ 2F_1^* F_2 - \cos \theta (F_1^* F_1 + F_2^* F_2) + \sin^2 \theta (F_1^* F_3 + F_2^* F_4) \} \rho \quad (26)$$

$$\hat{O}_{x'} = \sin \theta \text{Im} \{ F_2^* F_3 - F_1^* F_4 + \cos \theta (F_2^* F_4 - F_1^* F_3) \} \rho \quad (27)$$

$$\hat{O}_{z'} = -\sin^2 \theta \text{Im} \{ F_1^* F_3 + F_2^* F_4 \} \rho \quad (28)$$

$$\hat{L}_{x'} = -\sin \theta \text{Re} \{ F_1^* F_1 - F_2^* F_2 - F_2^* F_3 + F_1^* F_4 + \sin^2 \theta (F_4^* F_4 - F_3^* F_3) / 2 + \cos \theta (F_1^* F_3 - F_2^* F_4) \} \rho \quad (29)$$

$$\hat{L}_{z'} = \text{Re} \{ 2F_1^* F_2 - \cos \theta (F_1^* F_1 + F_2^* F_2) + \sin^2 \theta (F_1^* F_3 + F_2^* F_4 + F_3^* F_4) + \cos \theta \sin^2 \theta (F_3^* F_3 + F_4^* F_4) / 2 \} \rho \quad (30)$$

$$\hat{T}_{x'} = -\sin^2 \theta \text{Re} \{ F_1^* F_3 + F_2^* F_4 + F_3^* F_4 + \cos \theta (F_3^* F_3 + F_4^* F_4) / 2 \} \rho \quad (31)$$

$$\hat{T}_{z'} = \sin \theta \text{Re} \{ F_1^* F_4 - F_2^* F_3 + \cos \theta (F_1^* F_3 - F_2^* F_4) + \sin^2 \theta (F_4^* F_4 - F_3^* F_3) / 2 \} \rho, \quad (32)$$

where $\hat{\Sigma} = \Sigma \sigma_0$, etc. and $\rho = q/k$.

III. SINGLE-ENERGY SOLUTIONS

The SE solutions afford the most faithful description of the data, in terms of the lowest possible χ -squared,

spin observables	helicity representation	comparison with Fasano et al. [13]	comparison with Chiang et al. [15]
σ_0	$\frac{1}{2}(H_1 ^2 + H_2 ^2 + H_3 ^2 + H_4 ^2)$	$+\sigma_0$	$+\sigma_0 = +\tilde{\Omega}_1$
$\hat{\Sigma}$	$\text{Re}(H_1 H_4^* - H_2 H_3^*)$	$+\hat{\Sigma}$	$+\hat{\Sigma} = +\tilde{\Omega}_4$
\hat{T}	$\text{Im}(H_1 H_2^* + H_3 H_4^*)$	$+\hat{T}$	$-\hat{T} = +\tilde{\Omega}_{10}$
\hat{P}	$-\text{Im}(H_1 H_3^* + H_2 H_4^*)$	$+\hat{P}$	$+\hat{P} = +\tilde{\Omega}_{12}$
\hat{G}	$-\text{Im}(H_1 H_4^* + H_2 H_3^*)$	$+\hat{G}$	$-\hat{G} = -\tilde{\Omega}_3$
\hat{H}	$-\text{Im}(H_1 H_3^* - H_2 H_4^*)$	$-\hat{H}$	$-\hat{H} = -\tilde{\Omega}_5$
\hat{E}	$\frac{1}{2}(- H_1 ^2 + H_2 ^2 - H_3 ^2 + H_4 ^2)$	$-\hat{E}$	$-\hat{E} = -\tilde{\Omega}_9$
\hat{F}	$\text{Re}(H_1 H_2^* + H_3 H_4^*)$	$+\hat{F}$	$-\hat{F} = -\tilde{\Omega}_{11}$
$\hat{O}_{x'}$	$-\text{Im}(H_1 H_2^* - H_3 H_4^*)$	$-\hat{O}_{x'}$	$-\hat{O}_{x'} = -\tilde{\Omega}_{14}$
$\hat{O}_{z'}$	$\text{Im}(H_1 H_4^* - H_2 H_3^*)$	$-\hat{O}_{z'}$	$-\hat{O}_{z'} = +\tilde{\Omega}_7$
$\hat{C}_{x'}$	$-\text{Re}(H_1 H_3^* + H_2 H_4^*)$	$-\hat{C}_{x'}$	$+\hat{C}_{x'} = -\tilde{\Omega}_{16}$
$\hat{C}_{z'}$	$\frac{1}{2}(- H_1 ^2 - H_2 ^2 + H_3 ^2 + H_4 ^2)$	$-\hat{C}_{z'}$	$+\hat{C}_{z'} = -\tilde{\Omega}_2$
$\hat{T}_{x'}$	$\text{Re}(H_1 H_4^* + H_2 H_3^*)$	$+\hat{T}_{x'}$	$+\hat{T}_{x'} = -\tilde{\Omega}_6$
$\hat{T}_{z'}$	$\text{Re}(H_1 H_2^* - H_3 H_4^*)$	$+\hat{T}_{z'}$	$+\hat{T}_{z'} = -\tilde{\Omega}_{13}$
$\hat{L}_{x'}$	$-\text{Re}(H_1 H_3^* - H_2 H_4^*)$	$-\hat{L}_{x'}$	$+\hat{L}_{x'} = +\tilde{\Omega}_8$
$\hat{L}_{z'}$	$\frac{1}{2}(H_1 ^2 - H_2 ^2 - H_3 ^2 + H_4 ^2)$	$+\hat{L}_{z'}$	$-\hat{L}_{z'} = -\tilde{\Omega}_{15}$

TABLE I: Spin observables expressed by helicity amplitudes in the notation of Walker [10]. The sign definition is taken from Barker, Donnachie and Storrow [12] by replacing $N \rightarrow H_2$, $S_1 \rightarrow H_1$, $S_2 \rightarrow H_4$, $D \rightarrow H_3$ as given in the text. This sign definition is used by SAID and MAID. In column three, we compare the sign definitions of Fasano, Tabakin and Saghai [13], which is also used recently by Refs. [7, 14]. Furthermore we also give the sign definition of Chiang and Tabakin [15] and the relations to the Ω observables, that are the basis of the Fierz consistency relations given in Ref. [15].

consistent with constraints from the ED solutions. They have been used to probe the data for structure that may not have been properly encoded by the smooth ED solution. Both MAID and SAID SE solutions are determined by constrained fits to the data in sufficiently narrow energy bins. These constraints limit the variability in the SE results through the assumption that the global ED fit is close to the ‘true’ solution. This assumption appears to be validated by the fact that the χ -squared of both the ED and SE solutions suggest a realistic description of the data. Since the ED results are used to constrain the SE solutions in different ways within the MAID and SAID parametrization approaches, we begin this section with a brief description of their respective methods.

A. SAID SE Solutions

The SAID SE solutions are obtained in bins of the scattering energy spanning a few MeV. Starting values for the SE solutions are given by the multipole moduli and phases determined by ED solutions. In order to account for the variation of the modulus and phase over the width of an energy bin, a linear approximation to the energy dependence for each quantity is taken from the ED fit. The bin width increases from 5 to 20 MeV as the energy increases into regions with sparse measurements. Only the central values of the modulus and phase are searched for each SE solution; the slopes are held fixed. For the purposes of the present study, however, the pseudo data are generated at single energies coinciding with the central energy value of the bin. This removes the need to esti-

mate the energy variation based on an ED fit. In order to constrain the SE multipole solutions to be close to the ED values, the ED multipoles themselves are ascribed arbitrary errors and fitted along with experimentally determined reaction data of the bin under consideration. In general, these multipole ‘pseudo data’ contribute a negligible amount to the resultant chi-squared.

In all previously published sets of SE fits, the multipole phases were fixed to ED values when fitting to the data. As a result, multipole phases would change only through a modification of the ED fit. The number of searched multipoles has generally been subjective but may be increased until a χ^2/data near unity is approached.

As previously mentioned, the SAID SE fits were generated originally to search for structures not seen in the ED fit, and they have been used to re-initialize the ED fit, with the hope that this procedure would converge to the correct solution. As described above, they are not independent of the ED fit. It should be emphasized that the ED and SE solutions are fits to the experimentally observed reaction data; the ED solution is *not* a fit to the SE values.

B. MAID SE solutions

The MAID partial wave analysis follows a similar two-step approach[17]. In the first step, a global ED solution is determined first by fitting all experimentally observed reaction data, in a similar fashion to the SAID ED approach, in the range $140 \text{ MeV} \leq E_\gamma \leq 1610 \text{ MeV}$. This allows the determination of the phases of each mul-

tipole, i.e., the ratio $Im t_{\pi\gamma}^\alpha / Re t_{\pi\gamma}^\alpha$, where α is the multipole, above the two-pion threshold. At energies below the two-pion threshold, this phase is constrained, by Watson's theorem, to be equal to the πN scattering phase. In the second step we perform local SE fits to the data in energy bins of 10 MeV (over the range $140 \text{ MeV} \leq E_\gamma \leq 460 \text{ MeV}$) and 20 MeV (for the higher energies) by varying the absolute values of the multipoles but keeping the phase fixed. In order to damp strong local variations we introduce a penalty factor similar to a Bayesian approach and minimize the modified χ^2 function

$$\chi^2 = \sum_i^{N_{data}} \left(\frac{\Theta_i - \Theta_i^{exp}}{\delta\Theta_i} \right)^2 + \sum_j^{N_{mult}} \left(\frac{X_j - 1}{\Delta} \right)^2. \quad (33)$$

The first term on the right-hand side of this equation is the standard χ^2 function with Θ_i the calculated and Θ_i^{exp} the measured observables, $\delta\Theta_i$ the statistical errors, and N_{data} the number of data points. In the second term, N_{mult} is the number of the varied multipoles and X_j is the fitting parameter describing the deviation from the global fit, that is, the fitting procedure starts with the initial value $X_j = 1$ corresponding to the global solution, for each multipole indexed by j . The quantity Δ enforces a smooth energy dependence of the single energy solution. In the limit of $\Delta \rightarrow \infty$ we obtain the standard χ -squared, χ_{std}^2 , and for $\Delta \rightarrow 0$ the single energy and the global solutions become identical. The optimum value for Δ is chosen from the condition $1 < \chi^2 / \chi_{std}^2 < 1.05$. The described two-step fitting procedure may be repeated several times by adjusting the energy dependence of the global solution, for example by changing the resonance parametrization to obtain a better agreement between the global and local solutions.

IV. GENERATING PSEUDO DATA

Measurements of the spin observables defined in Sec. II C, over a large angular range with accuracy sufficient to have an impact on multipole analyses, require experiments of high intensity, with linearly and circularly polarized photon beams, strongly polarized targets and accurate recoil polarimetry together with hermetic detector systems. Such experiments have become technically possible only very recently at the tagged photon facilities at ELSA (University of Bonn), CEBAF (Jefferson Laboratory) and MAMI (University of Mainz).

For this study, we have generated pseudo data for single and double polarization observables of the $\gamma p \rightarrow \pi^0 p$ and $\gamma p \rightarrow \pi^+ n$ reactions with statistical uncertainties comparable to those expected at the above mentioned precision electromagnetic facilities within the next few years for energies from the reaction thresholds up to a photon beam energy of $E_\gamma = 1500 \text{ MeV}$ ($W = 1920 \text{ MeV}$)

Events for the neutral and charged pion reactions are generated via a Monte Carlo algorithm. A sample of reaction parameters – the beam energy, meson scattering angles (θ and ϕ), circular and linear beam polarizations, longitudinal and transverse target polarizations and the recoil nucleon spin alignment angles (θ_R and ϕ_R) – are drawn from a weight function given by the polarized cross section, Eq.(14)-(16). The events were generated for beam energy bins of $\Delta E_\gamma = 10 \text{ MeV}$ and angular bins of $\Delta\theta_\pi^{cm} = 10^\circ$, based on the MAID (MD07) model predictions. Beam polarizations are assumed to be $P_T = 60\%$ for linearly polarized photons and $P_\odot = 70\%$ for circularly polarized photons. These are typical values resulting from e^- to γ helicity transfer (giving circular photon polarization) and coherent bremsstrahlung (giving linear photon polarization), which are achieved at tagged photon facilities. We assume that the beam polarizations have no energy dependence and therefore should be interpreted as resulting from various sets of experimental conditions. For target protons an average polarization of $P = 80\%$ is assumed, as is available with butanol frozen spin targets [16]. The polarization of recoiling nucleons may be measured using a subsequent scattering reaction in a carbon analyzer. For these measurements an average analyzing power of $A = 20\%$ is assumed, close to values typically achievable. For each observable, typically $5 \cdot 10^6$ events have been generated over the full energy range. The pseudo data have not been folded with any additional acceptance given by a specific detector system.

The pseudo data are an accurate representation of both the MAID MD07 ED solution and the observed reaction data, as shown in Fig.(2). Here, the unpolarized cross section, $d\sigma/d\Omega$, the photon beam asymmetry, Σ , the target asymmetry, T , and the beam-target observable, G are shown at energies corresponding to the $\Delta(1232)$ resonance.

In the following section, we discuss the application of the SAID parametrization approach to obtain ED and SE solutions in fits to the pseudo data. We compare these solutions to the MAID MD07 ED solution and the pseudo data and discuss various features of their energy dependence.

V. DEPENDENCE ON ENERGY

Using the pseudo data generated from the MAID MD07 ED solution we apply the existing SAID parametrization approach[18, 19] to obtain the pion photoproduction multipoles. The results given below cover values of E_γ from 200 MeV to 1.2 GeV. The determination of a set of isospin-1/2 and 3/2 multipoles in the low-energy region is problematic due to the distinct thresholds for $\pi^0 p$ and $\pi^+ n$ photoproduction from the proton. We avoid this issue by fitting data above the $\pi^+ n$ threshold.

The use of Watson's theorem, greatly simplifies SE fits at energies where it is valid (depending on the multipole,

Multipole	SE4	MD07	SP09
$E_{0+}^{-1/2}$	9.40(0.08)	9.36	7.30
$E_{0+}^{3/2}$	18.06(0.16)	17.91	15.87
$M_{1-}^{1/2}$	2.28(0.15)	2.21	1.65
$M_{1-}^{3/2}$	9.26(0.27)	9.31	7.89
$E_{1+}^{-1/2}$	1.82(0.05)	1.79	1.76
$M_{1+}^{1/2}$	2.52(0.18)	2.55	1.99
$E_{1+}^{3/2}$	1.00(0.07)	1.12	1.08
$M_{1+}^{3/2}$	51.91(0.06)	52.0	55.25

TABLE II: Single-energy fit (SE4) to MD07 pseudo data compared to MD07 ED values at 340 MeV. The SP09 solution, fitted to the SAID database, is displayed for comparison. Multipoles given in millifermi units.

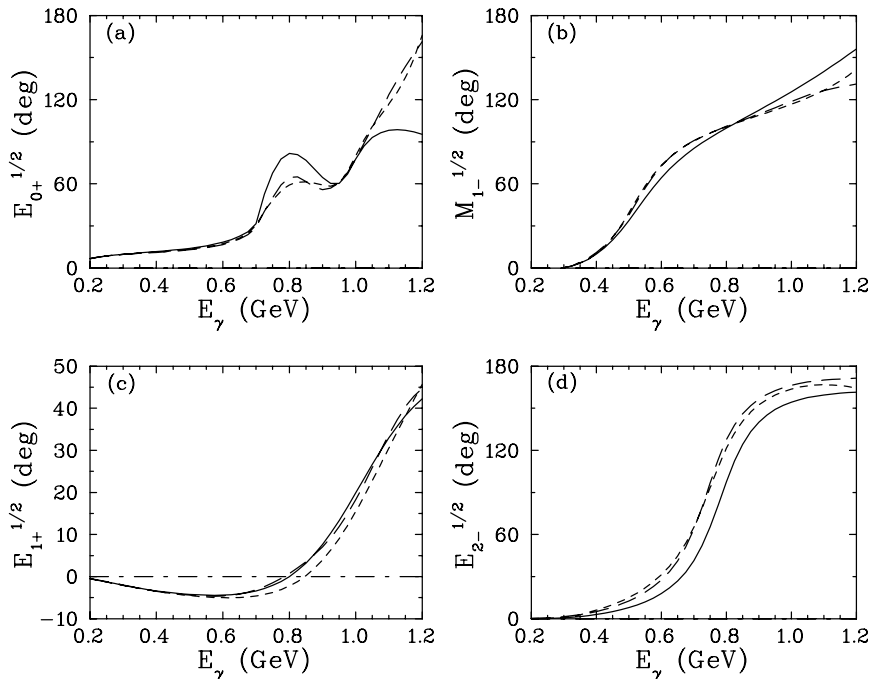


FIG. 6: Multipole phases from energy-dependent fits. SP09 (solid), MD07 (dashed), ED4 (dotted).

the Watson regime is typically somewhat higher than the first inelastic, two-pion threshold). Here, the multipole phase is fixed to the corresponding πN elastic partial wave phase and only the modulus allowed to vary. The SAID ED fit form, for each multipole, is

$$M = \alpha(1 + iT_{\pi N}) + \beta T_{\pi N} + \gamma(\text{Im}T_{\pi N} - |T_{\pi N}|^2), \quad (34)$$

$T_{\pi N}$ being the associated πN partial-wave amplitude, which allows a smooth transition from the Watson regime. Here α contains the Born contributions plus a (real) phenomenological term, β (also real) is purely phenomenological, and γ is a complex polynomial allowing a further departure from the Watson regime, proportional to the πN reaction cross section.

As shown in Table II, the SAID SE fit to MAID

pseudo data, at the $\Delta(1232)$ resonance energy ($E_\gamma = 340$ MeV), reproduces the dominant amplitudes. The SE result is, however, significantly different from an ED fit (SP09)[23] to the full SAID database of experimental observables, covering the resonance region. We note that this database, determining the SP09 solution, includes few measured polarization observables. In producing the SE result, SE4, only $d\sigma/d\Omega$, P , Σ , and T have been fitted.

In order to obtain an ED solution on which to base the SE solution of Table II, the SP09 solution was used as a starting point, from which a modified ED result was obtained from the fit to pseudo data, up to a photon energy of 1.2 GeV. A SE solution was then obtained, starting from ED, as described above. (Above, and in

Multipole	πN PW	MD07	SP09	ED4	SE4p	SE8p
$E_{0+}^{-1/2}$	S_{11}	16.7	18.4	17.4	16.0(3.0)	16.2(0.9)
$M_{1-}^{1/2}$	P_{11}	72.7	64.4	73.2	68.2(2.4)	73.4(1.6)
$M_{1-}^{3/2}$	P_{31}	163.9	167.1	172.0	176.8(6.5)	167.5(1.8)
$E_{2-}^{1/2}$	D_{13}	27.6	17.9	31.4	27.5(3.1)	26.1(1.0)
$M_{2-}^{1/2}$	D_{13}	26.8	22.2	26.7	25.5(1.8)	26.7(1.0)

TABLE III: Multipole phases (degrees) from single-energy fits to 4 (SE4p) and 8 (SE8p) observables at 600 MeV (phases searched), compared to the energy-dependent fits SP09, ED4, and MD07 (see text). Also listed is the associated πN partial wave (PW).

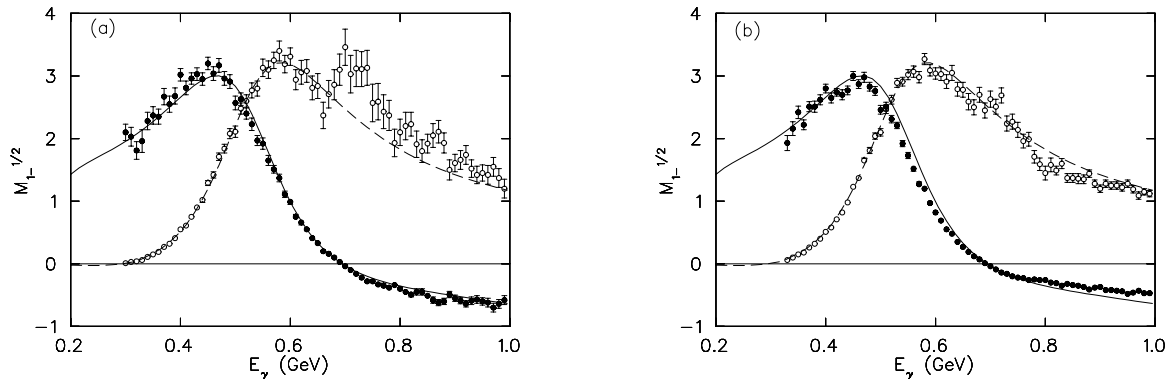


FIG. 7: Real and imaginary parts of the $P_{11}(pM)$ partial wave amplitude ($M_{1-}^{1/2}$). The solid (dashed) line shows the real (imaginary) part of the MD07 solution, used for the pseudo data generation. (a) Solid (filled) points display the SE4 fits to $d\sigma/d\Omega$ and the three single-spin observables Σ , T and P . (b) Notation as in (a) for SE8 fits also including the beam-target spin observables E , F , G and H . Standard SE fits displayed; phases not searched.

the following, the notation SE_n or ED_n denotes a fit to n observables.) We explore these solutions (the ED solution and its associated SE solutions) in detail below. The χ -squared for the resulting SE fit (SE4) at 340 MeV is 116 for 144 $d\sigma/d\Omega$, P , Σ , and T pseudo data. We note here, for subsequent discussion, that only the $\ell = 0, 1$ multipoles depart significantly from a Born approximation at the $\Delta(1232)$ resonance energy.

An alternative method that can be used at this energy, which reduces the influence of Watson's theorem, is to first fit the multipoles for π^+n photoproduction (both real and imaginary parts) for $\ell = 0, 1$, using the real Born multipoles for higher waves, to fix the overall phase. One can then fit the π^0p data separately, again fitting both the real and imaginary parts of contributing multipoles, with the $M_{1+}^{\pi^0p}$ multipole phase fixed, given the associated πN phase (by Watson's theorem, but in this P_{33} partial wave only) when combined with the previously determined $M_{1+}^{\pi^+n}$ multipole. This method requires fewer constraints, but results in multipoles with errors much larger than those given in Table II.

A form of this two-step method was used in an analysis by Grushin[20] and a recent update[21] and was found to give multipoles with phases consistent with Watson's theorem over the photon lab energy range of $280 < E_\gamma < 420$

MeV. As the P_{33} πN partial wave remains essentially elastic for CM energies $W \lesssim 1450$ MeV ($E_\gamma \lesssim 650$ MeV) the method could, in principle, be extended to this energy. This defines a second energy region, where not all multipoles have phases set by Watson's theorem, but reliable results can be obtained, with a self-consistent database of experimental reaction observables. A study by Omelaenko [22] suggests that the number of angular measurements required in order to determine multipoles up to a given angular momentum is of order 2ℓ for the differential cross section, and each single-polarization observable: P , Σ , and T . An additional double polarization measurement, such as F or G , is required to fix a remaining discrete ambiguity. Here we are fitting 18 angular pseudo data for each observable, which clearly exceeds the requirements given in Ref. [22]. Note also that the case considered in Ref. [22] was neutral pion photoproduction, and did not depend on the general use of Watson's theorem nor the charged-pion channel to determine the overall phase.

In Fig.(3), the SE and ED fits to pseudo data are compared to the cross section and single-spin asymmetries at 340 MeV. Agreement of the SE and ED solutions with the pseudo data for $d\sigma/d\Omega$ and the single-polarization observables, P , Σ , and T is obtained; agreement of the pre-

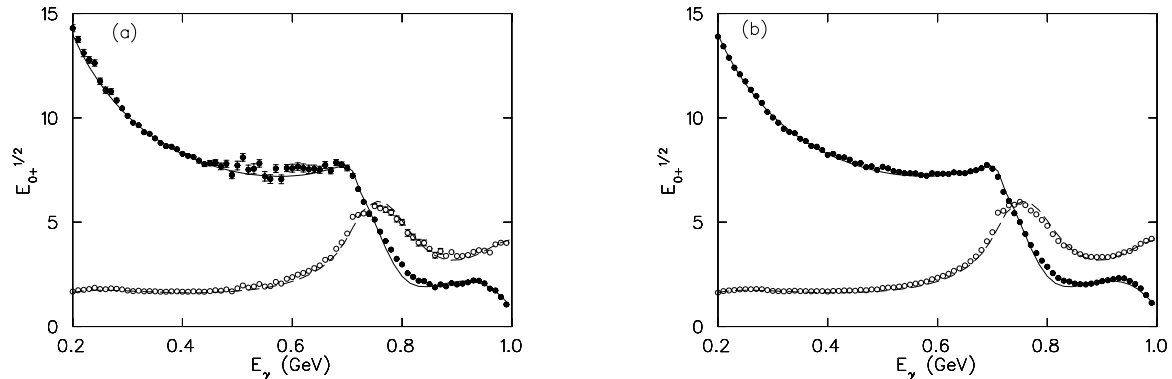


FIG. 8: Real and imaginary parts of the $S_{11}(pE)$ partial wave amplitude ($E_{0+}^{1/2}$). Notation as in Fig. 7.

dicted double-spin asymmetries (not shown) is obtained at a similar level. This has been accomplished without fitting the complete set of experiments required for amplitude reconstruction, as described in Ref. [15].

In Fig.(4), this process has been repeated at 600 MeV. The SE fit to $d\sigma/d\Omega$ and single-spin asymmetries (P , Σ , T) at this energy agree with the pseudo data, with a χ -squared of 89 for 144 data. At this photon (CM) energy, 600 MeV (1420 MeV), Watson's theorem is not generally valid in all multipoles. Inelasticity in the πN elastic P_{33} partial wave is, however, small up to 1450 MeV[4]. If we assume the $P_{33}(pM)$ ($M_{1+}^{3/2}$) multipole has the same phase as the πN elastic P_{33} amplitude and that the high partial waves for π^+n photoproduction are given by the Born terms, which are real, this should allow the reconstruction of all relevant multipoles. This was the approach taken in Ref.[21], although at lower energies than 600 MeV. This expectation is supported by Figs.(5) and (6) where the agreement between the displayed curves is of fair quality, though lower than that of the Fig.(4).

In Fig.(5), for example, the prediction for beam-target observables from the SE fit is compared to the pseudo data and the ED solution (ED4). The agreement is generally good but at the level of several standard deviations with respect to the pseudo data error bars at some angles. These discrepancies are reflected in the predicted multipoles[23].

The SAID SE procedure requires that the first ED fit to pseudo data provides the proper phases, as the subsequent SE search holds these phases constant. We can improve the agreement, however, by relaxing the phase constraint on the SE solution. In Fig.(6), we compare phases of the initial solution (SP09) to the ED re-fit (ED4), and the solution underlying the pseudo data (MD07). The agreement between MD07 and ED4 is generally good up to about 600 MeV, though there are very large differences between MD07 and SP09 in some multipoles.

In Table III, the phases of several multipoles are com-

pared at 600 MeV. Of particular interest are the multipoles $E_{0+}^{1/2}$ and $E_{2-}^{1/2}$, connected to the πN partial waves S_{11} and D_{13} , which are known to differ significantly between MAID and SAID, as can be seen comparing the values from MD07 and SP09. Note that the ED fit has improved the agreement, but does not match the phases for the D_{13} multipoles, as shown in Fig.(6), panel (d). The SE fit to cross section and polarization observables, displayed in Figs.(4) and (5), retains this phase mismatch. In the fit SE4p, the same set of four observables ($d\sigma/d\Omega$, P , Σ , T) is fitted, while allowing the multipole phases to vary; the result is tabulated in Table III. In SE8p, the set of fitted pseudo data has been expanded to contain beam-target double polarization quantities (E , F , G , and H), again allowing the phase to vary. By allowing phases to vary, we can now obtain a good reconstruction of the underlying model (MD07) for the dominant multipoles[23].

The 'standard' SE fit results (where the phases are not searched) are given for two multipoles in Fig.(7) and (8). The left and right panels display the effect of adding beam-target observables to the database. While uncertainties and scatter diminish with additional observables, some slight systematic deviations are visible. As described above, these can be reduced by allowing phase variation in the fit.

At much higher energies, where multipoles connected to the πN P_{33} partial-wave are no longer constrained in phase, the agreement deteriorates. However, the phase comparisons in Fig.(6) suggest that the ED re-fit to pseudo data generated from MD07 obtains the approximate phase of MD07 in many partial waves. It would be interesting to repeat this comparison with models other than MAID and SAID to better gauge the model-dependence of fit results at higher energies.

VI. CONCLUSION

We have performed ED and SE fits to realistic pseudo data generated from the MD07 ED multipole analysis over a range of photon (CM) energies from 200 (1120) to 1200 (1770) MeV. As a prelude, we have provided a detailed explanation of the amplitude definitions and the methods used in SE analysis by the MAID and SAID groups. This should be useful to those planning experiments and wishing to compare with the MAID and SAID predictions. It should also clarify the connections between SE and ED fits, and the data they analyze.

We have conducted a number of fits in order to explore the model-dependence of SE results in specific energy regions associated with pion photoproduction. Unlike the amplitude reconstruction process, which does not yield unique multipole solutions, the method described here appears to give good results with only fits to high-quality cross section and single-polarization data for energies where Watson's theorem is valid. A second re-

gion, extending over energies where the P_{33} πN amplitude remains elastic, has also been found to yield reproducible multipoles. At higher energies, results become more model-dependent, and further study is required to determine the reliability of SE multipoles determined via the methods described above.

Acknowledgments

This work was supported in part by the U.S. Department of Energy Grant DE-FG02-99ER41110, by the Deutsche Forschungsgemeinschaft (DFG) via the Sonderforschungsbereich SFB443 and the European Community-Research Infrastructure Activity under the FP6 (HadronPhysics, RII3-CT-2004-506078) and FP7 (HadronPhysicsII) programs. LT and MP wish to thank the European Centre for Theoretical Studies in Nuclear Physics for support during a portion of this project.

-
- [1] T.P. Vrana, S.A. Dytman, T.S.H. Lee, Phys. Rept. **328**, 181 (2000); T. Feuster and U. Mosel, Phys. Rev. **C59**, 460 (1999); A.M. Green and S. Wycech, Phys. Rev. **C60**, 035208 (1999).
 - [2] R.A. Arndt, I.I. Strakovsky, R.L. Workman, Phys. Rev. **C62**, 034005 (2000); J. Bystrický, C. Lechanoine-Leluc, F. Lehar, Eur. Phys. J. **C4**, 607 (1998).
 - [3] I.G. Alekseev, V.P. Kanavets, B.V. Morozov, D.N. Svirida, S.P. Kruglov, A.A. Kulbardis, V.V. Sumachev, R.A. Arndt, I.I. Strakovsky, R.L. Workman, Phys. Rev. **C55**, 2049 (1997).
 - [4] R. A. Arndt, W. J. Briscoe, I. I. Strakovsky *et al.*, Phys. Rev. **C74**, 045205 (2006).
 - [5] K. Nakamura *et al.* [Particle Data Group Collaboration], J. Phys. G **G37**, 075021 (2010).
 - [6] A. M. Sandorfi, S. Hoblit, H. Kamano and T. S. Lee, arXiv:1010.4555 [nucl-th].
 - [7] B. Dey, M. E. McCracken, D. G. Ireland *et al.*, [arXiv:1010.4978 [hep-ph]].
 - [8] G.F. Chew, M.L. Goldberger, F.E. Low, and Y. Nambu, Phys. Rev. **106**, 1347 (1957).
 - [9] L.D. Pearlstein and A. Klein, Phys. Rev. **107**, 836 (1957).
 - [10] R.L. Walker, Phys. Rev. **182**, (1969) 1729.
 - [11] I. S. Barker, A. Donnachie, J. K. Storrow, Nucl. Phys. **B79**, 431 (1974).
 - [12] I.S. Barker, A. Donnachie, J.K. Storrow: Nucl. Phys. **B 95**, (1975) 347.
 - [13] C.G. Fasano, F. Tabakin, B. Saghai: Phys. Rev. **C 46** (1992) 2430.
 - [14] A. V. Anisovich, E. Klempt, V. A. Nikonov *et al.*, Eur. Phys. J. **A44**, 203-220 (2010).
 - [15] W.-T. Chiang and F. Tabakin, Phys. Rev. **C 55**, 2054 (1997).
 - [16] S. Goertz, W. Meyer and G. Reicherz Prog. Part. Nucl. Phys. **49**, (2002) 403.
 - [17] D. Drechsel, S. S. Kamalov, L. Tiator, Eur. Phys. J. **A34**, 69-97 (2007).
 - [18] R. A. Arndt, R. L. Workman, Z. Li *et al.*, Phys. Rev. **C42**, 1853-1863 (1990).
 - [19] R. A. Arndt, I. I. Strakovsky, R. L. Workman, Phys. Rev. **C67**, 048201 (2003).
 - [20] V.F. Grushin, in *Photoproduction of Pions on Nucleons and Nuclei*, edited by A.A. Komar (Nova Science, New York, 1989), p. 1ff.
 - [21] R. L. Workman, [arXiv:1007.3041 [nucl-th]].
 - [22] A.S. Omelaenko, Sov. J. Nucl. Phys. **34**, 406 (1981).
 - [23] Results presented in the present publication, and some additional, related work, may be obtained online at <http://gwdac.phys.gwu.edu/analysis/go56pr.html>.